Neuronal Oscillatory Signatures in the Developing Mouse Visual Cortex After Short-Term Monocular Deprivation

Malik, Anju; Eldaly, Abdelrahman B. M.; Chen, Ke; Chan, Leanne Lai-Hang

Published in:
Cerebral Cortex

Published: 15/06/2022

Document Version:
Post-print, also known as Accepted Author Manuscript, Peer-reviewed or Author Final version

Published version (DOI):
10.1093/cercor/bhab372

Publication details:
Malik, A., Eldaly, A. B. M., Chen, K., & Chan, L. L.-H. (2022). Neuronal Oscillatory Signatures in the Developing Mouse Visual Cortex After Short-Term Monocular Deprivation. *Cerebral Cortex*, *32*(12), 2657-2667. https://doi.org/10.1093/cercor/bhab372

Neuronal oscillatory signatures in the developing mouse visual cortex after short-term monocular deprivation

Anju Malik[1], Abdelrahman B. M. Eldaly[1], Ke Chen[3], and Leanne Lai-Hang Chan[1,2],

[1]Department of Electrical Engineering, City University of Hong Kong, Hong Kong SAR

[2]Center for Biosystems, Neuroscience, and Nanotechnology, City University of Hong Kong, Hong Kong SAR

[3]Sichuan Provincial People's Hospital, School of Medicine, University of Electronic Science and Technology of China, Chengdu 610072, China

Corresponding author:

Dr. L.L.H. Chan, Associate Professor

Department of Electrical Engineering & Center for Biosystems, Neuroscience, and Nanotechnology, City University of Hong Kong, Hong Kong SAR

Phone: +852-34429120; Fax: +852-34420562; e-mail address: leanne.chan@cityu.edu.hk

Abstract

Development and maturation in cortical networks depend on neuronal activity. For stabilisation and pruning of connections, synchronised oscillations play a crucial role. A fundamental mechanism that enables coordinated activity during brain functioning is formed of synchronised neuronal oscillations in low (delta and theta) and high (gamma) frequency bands. The relationship between neural synchrony, cognition, and the perceptual process has been widely studied, but any possible role of neural synchrony in amblyopia has been less explored. We hypothesised that monocular deprivation (MD) during early postnatal life would lead to changes in neuronal activity that would be demonstrated by changes in phase-amplitude coupling (PAC) and altered power in specific oscillatory frequency. Our results demonstrate that functional connectivity in the visual cortex is altered by MD during adolescence. The amplitude of high-frequency oscillations is modulated by the phase of low-frequency oscillations. Demonstration of enhanced delta-gamma and theta-gamma PAC indicates that our results are relevant for a broad range of nested oscillatory markers. These markers are inherent to neuronal processing and are consistent with the hypothesised increase in the intrinsic coupling that arises from neural oscillatory phase alignment. Our results reveal distinct frequency bands exhibit altered power and coherence variations modulated by experience-driven plasticity.

Keywords— Cortical plasticity, critical period (CP), experience-dependent plasticity, phase-amplitude coupling (PAC), neuronal oscillations

I. INTRODUCTION

Brain functions entail the continual synchronisation and desynchronisation of neuronal ensembles at various oscillatory frequencies. These ensembles communicate with each other to integrate their local information flows into a common brain network (Buzsaki and Draguhn 2004). Often, electrophysiological brain oscillations are separated into distinct frequency bands that range from low-frequency delta (1-4 Hz) to high-frequency gamma (< 40 Hz) bands. Alterations in the signal power of these frequency bands are linked to periodic neural activity (Gao 2016). This relationship between signal power and neural activity has been shown to be a powerful tool in neuroscientific research. Meanwhile, there is emerging evidence that high-frequency activity in the local field potential (LFP) is modulated by the phase of low-frequency oscillations. This phenomenon, known as phase-amplitude coupling (PAC), has been well documented in both human and animal studies. Visual stimuli modulate the amplitude of the activity-induced ongoing oscillations in the visual cortex (V1) (Berens et al. 2008; Katzner et al. 2009) and lead to coupling of gamma oscillations and spike rates with the phase of slower rhythms (Rasch et al. 2008; Whittingstall and Logothetis 2009). This developmental change is modulated by visual behavioural tasks, by the increased power of high gamma frequencies (80-150 Hz), and by the phase of slow oscillations (Canolty et al. 2006; Bruns and Eckhorn 2004; Demiralp et al. 2007). Also, there is strong evidence that dynamic coupling occurs between the delta phase (1-5 Hz) and gamma amplitude (> 40 Hz) frequencies and the rhythm of the stream, which serves as an instrument of sensory selection (Lakatos et al. 2008).

Intriguingly, these couplings have been proposed to act as mechanisms for the dynamic coordination of brain activity over multiple spatial scales within the visual system (Bonnefond and Jensen 2015). Such action would enable the efficient routing of information between regions of

plasticity during the critical period (CP) of development and the segmentation and maintenance of neuronal representation (Bonnefond and Jensen 2015). The CP is the period in early postnatal life during which plasticity is enhanced and neural circuits display heightened sensitivity to acquire instructive and adaptive signals from the external environment. Neurophysiological changes accompany functional plasticity in the developing V1 of the mouse, as they do in higher mammals (Antonini, Fagiolini, and Stryker 1999). In rodents, changes in gamma rhythm have been observed to correlate with CP plasticity. During the CP, eyelid closure drives a robust, transient peak in gamma power (Lensjo et al. 2017). Both the generation of this oscillatory activity (Sohal et al. 2009; Bartos, Vida, and Jonas 2007) and CP plasticity are dependent on the level of inhibition in the circuit. The enhancement of PAC of the deprived eye during CP monocular deprivation (CPMD), is suggestive of the formation and strengthening of new synchronous neural connections in the non-deprived eye. MD is achieved by the suturing of the eyelid of one eye to induce experience-driven plasticity in the mouse visual cortex. Thus, the emergence of neuronal oscillations during CP plasticity in the V1 requires explicit investigation.

In the study that is explained here, we investigated the coupling between different frequency bands, by comparing the response of both the deprived and non-deprived eyes towards the same visual stimuli in the primary V1 of an anaesthetised mouse. We found a relationship between low-frequency oscillations (LFOs) and high-frequency oscillations (HFOs) during juvenile CPMD and dissociation of both in wild-type (WT) adult mice with MD. We focused on the delta-to-gamma phase and theta-to-gamma phase interactions during MD. Moreover, our results clearly show the difference in the form of coupling function that occurs in juvenile mice with CPMD compared with WT adult mice with MD. This work paves the way to further applications and advancement of the understanding of brain function. During juvenile CPMD, cross-frequency coupling between

low (i.e. delta and theta) and high (e.g. low to ultra-high gamma) frequencies results in drastic fluctuations. Also, alterations in the LFP power bands (delta, theta, alpha, and gamma) are seen in the non-deprived eye compared with the deprived eye. In contrast, in WT adult MD, the deprived eye shows the emergence of delta and theta LFP power bands compared with the non-deprived eye. Furthermore, the change in coherence between populations of neurons residing at different depths in the V1 is seen between the WT adult MD and juvenile CPMD mice. Thus, experience-dependent plasticity is found to modulate neuronal oscillations in an eye-specific manner in the V1 as defined by the information that is contained in different power bands.

II. MATERIALS AND METHODS

A. Animals and experimental groups

Adult male/female wild-type (C57BL/6) mice (n = 10) were used. In-house animal breeding was performed in the Laboratory Animal Research Unit at the City University of Hong Kong. The mice were kept under conditions of a 12hour:12hour light/dark cycle and were housed in individually ventilated cages. Five mice were housed in each cage and were allowed free access to food and water. All experimental protocols were approved by the animal research ethics sub-committees of the City University of Hong Kong and the Department of Health, Hong Kong Special Administrative Region. Five mice in each group WT adult (P60) and CP (P23), were used for the experiments.

B. Short-term monocular deprivation

For short-term MD (4-days), a number of animals were deprived for varying lengths of time, all centered around P28 and P65. One eye was closed on postnatal day 23 in the juveniles and on P60 in the adults. The procedure was conducted through the application of a single suture that was tied

with a 6-0 nylon surgical suture needle with thread (Ningbo Medical Needle Co. Ltd, China). The mice were placed under brief anaesthesia through the use of a ketamine–xylazine (K-X) combination (ketamine, 100mg/kg; xylazine, 10 mg/kg; Alfasan International B.V., Holland). MD in all the animals was conducted with 4 days' eyelid closure. The sutures were removed with fine iridectomy scissors 4 days later and the eyes were flushed with sterile saline. The eyes were examined and animals whose corneas showed signs of scarring were eliminated from the study.

C. Surgical procedure

The mice were anaesthetised through the application of a K-X combination during the surgical preparation. The body temperatures of the mice were maintained at 37°C by use of a homeostatically controlled heating pad during the surgery. Following the induction of anaesthesia, each mouse was mounted on a stereotaxic instrument (RWD Life Science, Shenzhen, China) and an incision was made along the midline of the head. The stereotaxic instrument was adjusted to place the bregma and lambda points of the skull on a flat skull surface (anteroposterior (AP): -3.2 mm to -4.0 mm; mediolateral (ML): 3.0 mm to 3.8 mm, relative to bregma). A piece of the scalp over the V1 was removed to expose the cortex, and a bone screw was fixed in the frontal bone as the reference electrode. The exposed cortical surface was then covered with extracellular saline (in mM: 125 NaCl, 5 KCl, 10 glucose, 10 4-(2-hydroxyethyl)-1-piperazineethanesulphonic acid (HEPES), and 2 $CaCl_2$; pH adjusted to 7.4) to prevent drying of the surface. The electrode was lowered into the brain to an appropriate depth (V1 < 1mm) and was allowed to settle for 30 minutes before recording was begun. In each mouse, three to four separate penetrations were spaced evenly at least 200 μm apart across the binocular region of V1. The eyes were kept moist with ophthalmic lubricant ointment until recording to prevent drying while enabling clear optical transmission. At

the end of the recording, the mice were euthanised by injection of an overdose of Dorminal (300mg/kg).

D. Visual stimuli

The visual stimulus was generated with a Matlab (R2012b) script that was based on a package called Psychtoolbox-3 (PTB-3) (Brainard, 1997) on a liquid crystal display monitor with a light-emitting diode backlight (P2311Hb, Dell, United States). Receptive fields of isolated single units were plotted by use of a monitor that was placed 25 cm in front of the animal's eyes at an angle of 53° from a line that extended from the animals' midline. Bars of light were varied in size and orientation, in appropriate cases, to obtain a maximal response; for those cells that showed orientation selectivity, the preferred orientation was noted. Cells within the central 30-40° of the upper portion of each hemifield could receive input from both eyes (Gordon and Stryker 1996). The binocular zone was defined as the central 25° of each visual hemifield. The vertical meridian was defined as the intersection of the midline of the animal with the tangent screen. In the case of spatial acuity, visual stimuli of sinusoidal drifting gratings of increasing orientation angles (0-330°) were supplied at a rate of 0.04 cycles per degree (cpd) in random order and were repeated for 10 cycles. The movie duration was 1.5 s drifting sinusoidal grating and 1 s break at temporal frequency 2 Hz. Optimal stimuli were presented to each eye alternately, and the relative strength of the response was determined.

E. Local field potential recording

Recordings were performed with the use of a polyimide-coated platinum/iridium (70:30) ribbon microelectrode array (Clunbury Scientific LLC, United States), as shown in Fig. 1. The tip resistances were 30-50 kΩ. The A-M Systems 3600 (A-M Systems, United States) and CED Micro 1401-3 (Cambridge Electronic Design, United Kingdom) instruments were used as the amplifier

and data acquisition system, respectively. The signals were sampled at 25 kHz and band-pass-filtered at 0.3-300 Hz for LFP, amplified, and fed to spike2 software (Cambridge Electronic Design, United Kingdom) and the Matlab program for offline analysis. The raw data were first converted to a Matlab-compatible format. A notch filter was applied off-line to the LFP signals to remove the 50 Hz noise of the power line. Thus, in one recording session, we sampled neuronal signals from 16 recording sites in V1.

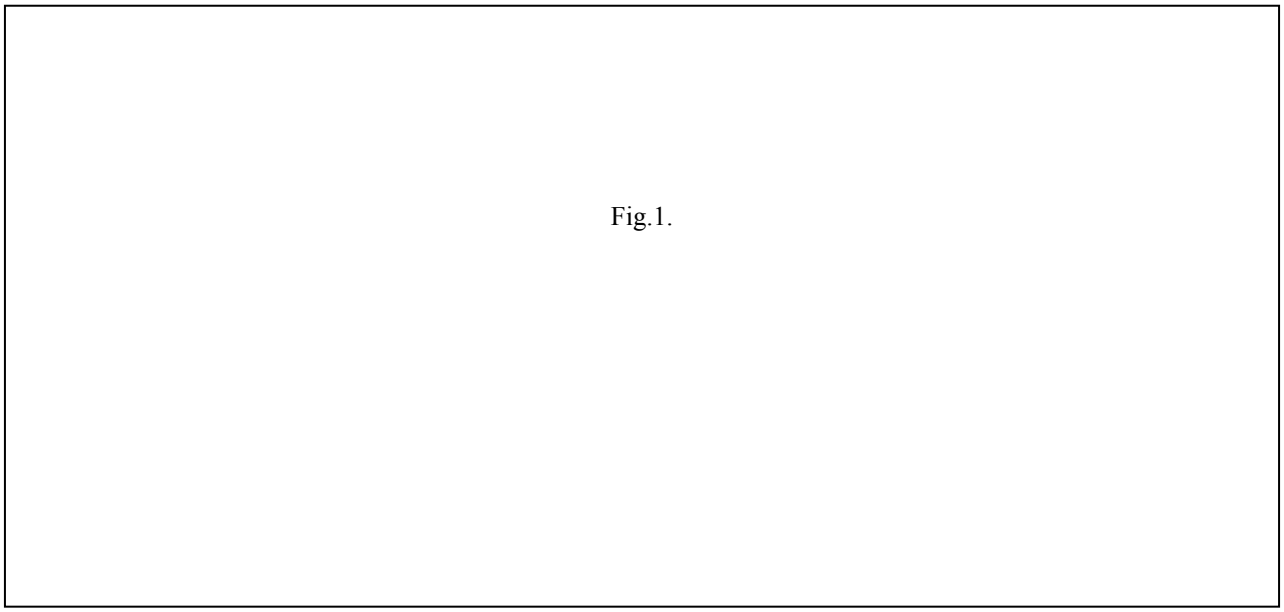

F. The modulation index and the phase-to-amplitude comodulogram

To assess the influences on neural oscillatory synchrony after four days of MD during the CP in mice, cross-frequency coupling (CFC) between LFOs and HFOs was analysed by use of the PAC method, and the modulation index (MI) was computed based on the Kullback-Leibler MI estimation (Tort et al. 2010). Firstly, the raw data were filtered by use of a linear finite impulse response (FIR) filter into a lower-frequency band (1-29 Hz) for the phase and a higher-frequency band (10-300 Hz) for the amplitude. For each filtered signal, the time series of the phases of a lower-frequency band and the amplitude envelope of a higher-frequency band of the LFP signal were extracted by application of the standard Hilbert transform. Secondly, the phases were

categorised into 18 interval bins (from 0^0 to 360^0 with steps of 20^0). The mean of the amplitude envelope over each phase bin was calculated to quantify the amplitude distribution over phase bins. Lastly, the MI was computed by normalisation of H (the entropy measure of the normalised amplitude distribution over phase bins) by application of the maximum possible entropy value Hmax = log(N), where N was equal to the number of phase bins, as follows:

$$MI = \frac{H\_max - H}{H\_max} \quad (1)$$

The average MI was calculated for all trials in each group. The comodulogram plot was obtained by the representation of the average MI values of multiple phases and amplitude-frequency pairs. These were calculated in 1 Hz steps with 2 Hz bandwidths for phase and 2 Hz steps with 4 Hz bandwidths for amplitude. The 8 different types of CFC were investigated between the two phase-frequency bands [delta (0.5-5 Hz), and theta (5-10 Hz)] and four amplitude-frequency bands [low gamma (30-55 Hz), medium gamma (60-115 Hz), high gamma (125-175 Hz), and ultra-gamma (185-300 Hz)]. To test the statistical significance of the MI values, a distribution of 50 surrogate MI values was created by random shuffling of the composite time series of high-frequency amplitude envelopes and phases of a low-frequency signal after segmentation into 20 equal blocks. Assuming the surrogate MI values were normally distributed, the MI value of the original signal was considered significant if it reached the top 5 % of this distribution of surrogate data; otherwise, it was ignored and replaced with zero. In other words, in the comodulogram plots, any MI value that was greater than zero was statistically significant. The MI values were then computed for all mice between CE and IE across the two groups (WT adult MD and juvenile CPMD mice).

G. Power spectrum analysis

The power spectrum of the spontaneous LFP was computed through the use of the multi-taper estimation method in Matlab with the chronux package. Then, the spectrum was smoothed by

using the "locfit" function (provided by the chronux toolbox) after line noise had been removed (50 Hz) to reduce the variation without destroying the features (Chen et al. 2015). Finally, the power was normalised to the mean power across all frequency bands (0.5-300 Hz).

H. Coherence analysis

The coherence between the contralateral eye (CE) and ipsilateral eye (IE) was calculated by the magnitude squared of coherence C_{xy}. This gives an estimated coherence value of the input signal x and y using the method of Welch's average modified periodogram method. It is important to note that $C_{xy}(f)$ acts as a function of frequency and has values ranging from 0 to 1 which is an indication of the extent to which x correlates with y per frequency.

$$C_{xy}(f) = \frac{|P_{xy}(f)|^2}{P_{xx}(f)P_{yy}(f)} \qquad where \quad 0 \leq C_{xy}(f) \leq 1 \tag{2}$$

In Eq. (2) above, $P_{xx}(f)$ and $P_{yy}(f)$ represent the power spectral density of x and y and $P_{xy}(f)$ represents the cross-power spectrum spectral density. Subsequently, $C_{xy}(f)$ was estimated at each epoch and frequency bin over the entire 0.5–300 Hz frequency range for each mouse. The LFP channel was sliced into 2-s epochs with 50% overlapping between every two adjacent epochs over the entire LFP recording. For each eye, the average coherence is calculated across all possible channel pairs (120 pairs). The mean coherence for 16 LFP channels were then computed for all mice between CE and IE across the two groups (WT adult MD and juvenile CPMD mice).

I. Statistical analysis

The number of electrode sites (LFP files) used for the group WT adult MD (P60-P65) and juvenile CPMD (P23-P28) were 128 and 137 respectively. Statistical analysis was performed through the use of GraphPad prism software version 8.0.1. All p-values were determined with paired 't' tests except otherwise stated.

III. RESULTS

A. Phase-to-amplitude modulations during critical period monocular deprivation

The change in neural oscillatory synchrony between LFOs (delta, theta) and HFOs (gamma) of the V1 after four days of MD in the juvenile and WT adult mice was tested by evaluating the PAC of respective oscillations, and through calculation of the mean MI (Table 1).

During four days of MD in the WT adult animals, a PAC between delta-gamma and theta-gamma oscillations was observed (Table 1). To investigate further the effect of MD on neuronal oscillatory synchrony in the IE and CE, the MI was compared between the eyes. No significant difference in MI±SEM was observed between the IE and the CE (delta-gamma, IE vs. CE, 4.555±0.525 vs. 4.504±0.406 $x10^{-3}$, $p>0.05$). Similarly, no significant difference in MI±SEM was observed between the IE and the CE (theta-gamma, IE vs. CE, 0.058±0.000 vs. 0.051±0.000 $x10^{-3}$, $p>0.05$). Plasticity in V1 had ceased in adulthood, and it was not altered by the imposition of MD in one eye, which is well-documented in early studies (Guire, Lickey, and Gordon 1999; Sawtell et al. 2003; Tagawa et al. 2005).

In contrast, in juvenile CPMD, a PAC between delta-gamma and theta-gamma oscillations was observed (Table 1). The effect of MD on neuronal oscillatory synchrony was investigated further in the IE and the CE. A significant increase in MI±SEM was observed in the IE compared with the CE (delta-gamma, IE vs. CE, 6.634±0.400 vs. 4.722±0.226 $x10^{-3}$, $p<0.01$; theta-gamma, IE vs. CE, 4.597±0.035 vs. 2.543±0.021 $x10^{-3}$, $p<0.01$). It is known that CPMD leads to neuroplasticity changes in the V1 and a shift in the eye response towards the non-deprived eye (IE) from single-unit or multiunit recordings (Gordon and Stryker 1996; Issa et al. 1999; Fagiolini et al. 1994). Our results, which show coupling between delta-gamma and theta-gamma oscillations, provide an insight into the neuronal oscillatory synchrony of V1 neurons during CPMD. This finding also

243 provides an understanding of the role of oscillatory rhythms in low and high-frequency ranges in
244 the establishment of precise synchronisation of neuroplasticity changes in the V1 after MD.

245

246 *B. The intensity of amplitude modulation may correlate with monocular deprivation*

Table 1.

247 To determine the frequency bands that were involved in the PAC, a comodulogram plot was
248 constructed, which depicts the MI value between LFOs and HFOs on a heat map (Fig. 2). In WT
249 adult mice that had undergone MD for four days, the amplitude of the gamma HFOs was
250 modulated by the phase of the delta LFOs in both the CE and the IE (Fig. 2a). In juvenile CPMD
251 mice, the amplitude of the gamma HFOs was similarly modulated by the phase of the delta LFOs
252 in both the CE and the IE (Fig. 2b, dotted white box). However, the amplitude of the gamma HFOs
253 was also modulated by the phase of the theta LFOs in both the CE and the IE (Fig. 2b, dotted black
254 box). Hence, a comodulogram plot demonstrates that juvenile CPMD displays enhanced neural
255 oscillatory synchrony as compared with WT adult MD.

Fig.2.

C. Possible cross-frequency interactions of low-frequency bands with different gamma bands

We measured the coupling of delta and theta oscillations with different gamma bands of the V1. The MI was calculated across eight different frequency combinations: low-frequency (delta (0.5-5 Hz), and theta (5-10 Hz)) and high-frequency gamma1 (30-55 Hz), gamma2 (60-115 Hz), gamma3 (125-175 Hz), and gamma4 (185-300 Hz) were compared between the IE and the CE (Fig. 2c, d).

After four days of MD in WT adult mice, firstly the MI±SEM of the IE was compared with that of the CE between delta and gamma1 (IE vs. CE, 1.109±0.136 vs. 1.127±0.152 $x10^{-2}$, $p>0.05$), gamma2 (IE vs. CE, 3.012±0.263 vs. 3.469±0.247 $x10^{-3}$, $p>0.05$), gamma3 (IE vs. CE, 1.790±0.121 vs. 1.899±0.087 $x10^{-3}$, $p>0.05$) and gamma4 (IE vs. CE, 2.196±0.019 vs. 1.731±0.089 $x10^{-3}$, $p>0.05$), as shown in Fig. 2c (*top*). No significant differences in the MI were observed between the IE and the CE in the coupling of the delta with different gamma bands. Secondly, the MI±SEM of the IE was compared with that of the CE between theta and gamma1 (IE vs. CE, 0.442±0.041 vs. 0.669±0.089 $x10^{-3}$, $p>0.05$), gamma2 (IE vs. CE, 0.579±0.050 vs. 1.229±0.090 $x10^{-3}$, $p>0.05$), gamma3 (IE vs. CE, 0.511±0.020 vs. 0.952±0.048 $x10^{-3}$, $p>0.05$) and gamma4 (IE vs. CE, 0.393±0.038 vs. 0.596±0.052 $x10^{-3}$, $p>0.05$). No significant differences in MI were found between the IE and the CE in the coupling of theta with different gamma bands (Fig. 2c, *bottom*).

In juvenile CPMD mice, firstly the MI±SEM of the IE was compared with that of the CE between delta and gamma1 (IE vs. CE, 5.815±0.411 vs. 3.945±0.373 $x10^{-3}$, $p<0.01$), gamma2 (IE vs. CE, 9.357±0.676 vs. 7.313±0.375 $x10^{-3}$, $p<0.01$), gamma3 (IE vs. CE, 8.140±0.515 vs. 5.571±0.251 $x10^{-3}$, $p<0.01$) and gamma4 (IE vs. CE, 3.225±0.185 vs. 2.070±0.183 $x10^{-3}$, $p<0.05$). The MI of the delta with all gamma bands was significantly higher in the IE than in the CE, as shown in Fig.

2d (*top*). Secondly, the MI±SEM of the IE was compared with that of the CE between theta and gamma1 (IE vs. CE, 1.353±0.237 vs. 0.837±0.140 x10^{-3}, p>0.05), gamma2 (IE vs. CE, 6.118±0.466 vs. 3.861±0.305 x10^{-3}, p<0.001), gamma3 (IE vs. CE, 6.321±0.345 vs. 2.931±0.199 x10^{-3}, p<0.001) and gamma4 (IE vs. CE, 1.003±0.136 vs. 0.735±0.006 x10^{-3}, p>0.05). The MI of theta with medium gamma and high gamma oscillations was significantly higher in the IE than in the CE (Fig. 2d, *bottom*). No significant differences in MI were found between the IE and the CE in the coupling of theta with low and ultra-high gamma oscillations. Our results demonstrate that the experience-dependent plasticity that was induced by CPMD was characterised by the change in the coupling between low- and high-frequency synchrony, but not in WT adult MD.

D. Distinct frequency bands exhibit different power variations during juvenile critical period monocular deprivation

The LFP power spectrum is a measure of the variance in the signal as a function of frequency and is related to the time domain signals through the Fourier transform of the autocorrelation function (Henrie and Shapley 2005). The changes were considered in the LFP power spectrum across different frequency bands, namely delta (0.5-5 Hz), theta (5-10 Hz), alpha (10.5-15 Hz), beta (15-30 Hz), and gamma (30-300 Hz) of the V1 after four days of MD in the juvenile and WT adult animals (Fig. 3). The mean power (MP) was calculated (MP±SEM) and compared between the IE and the CE.

After four days of MD in WT adult mice, the MP±SEM of the IE was compared with that of the CE. Significant increase of the mean power in the CE than in the IE were observed in delta (IE vs. CE, 30.650±2.964 vs. 36.150±3.181, p<0.05), as shown in Fig. 3a and theta (IE vs. CE, 1.017±0.062 vs. 1.234±0.086, p<0.05), as shown in Fig. 3b frequency bands. No significant differences in the mean power were found between IE and CE in the alpha (IE vs. CE, 0.345±0.024

303 vs. 0.386±0.027, p>0.05), as shown in Fig. 3c, beta (IE vs. CE, 0.433±0.031 vs. 0.473±0.033,
304 p>0.05), as shown in Fig. 3d and gamma (IE vs. CE, 1.240±0.081 vs. 1.323±0.088, p>0.05), as
305 shown in Fig. 3e, frequency bands.
306 In juvenile CPMD mice, the MP±SEM of the IE was compared with that of the CE. Significant
307 increases of the mean power in the IE than in the CE were observed in the delta (IE vs. CE,
308 10.990±1.118 vs. 7.996±1.119, p<0.05) in Fig. 3a, theta (IE vs. CE, 1.328±0.141 vs. 0.844±0.091,
309 p<0.01) in Fig. 3b, alpha (IE vs. CE, 0.877±0.079 vs. 0.564±0.046, p<0.01) in Fig. 3c and gamma
310 (IE vs. CE, 3.803±0.393 vs. 2.880±0.249, p<0.01), in Fig. 3e, frequency bands. No significant
311 differences in the mean power were found between IE and CE in the beta (IE vs. CE, 1.239±0.130
312 vs. 1.036±0.116, p>0.05), in Fig. 3d, frequency band. The shift in eye response towards the IE
313 from CE was possibly due to the occurrence of plasticity during the CPMD as observed in juvenile
314 CPMD.

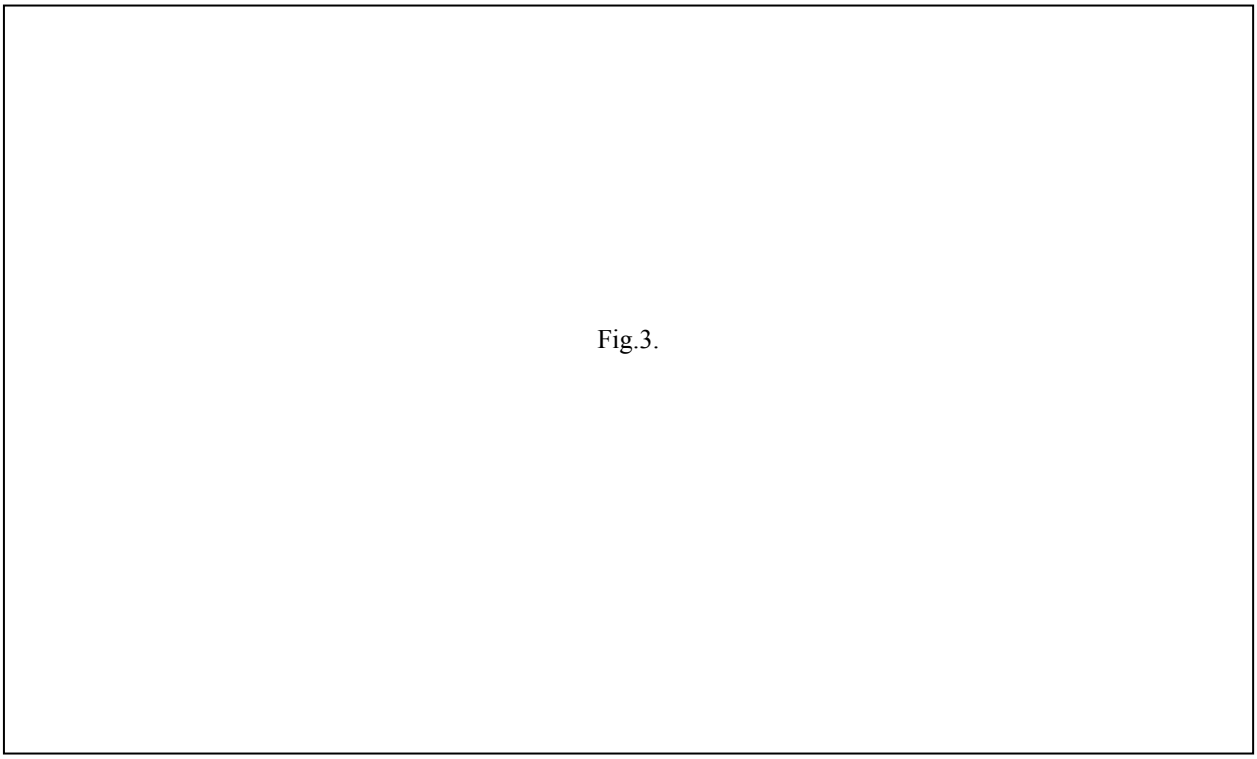

Fig.3.

315

316 *E. Coherence modulations during critical period monocular deprivation*

317 The LFP coherence provides the functional interactions between neural systems operating in each
318 frequency band (Buzsaki and Schomburg 2015; Srinath and Ray 2014). The change in coherence
319 between populations of neurons residing at different depths (100-700 μm) was measured between
320 the IE and the CE in WT adult MD and juvenile CPMD mice across eight different frequency
321 bands, namely low-frequency bands including delta (0.5-5 Hz), theta (5-10 Hz), alpha (10.5-15
322 Hz) and beta (5-30 Hz) and high-frequency bands including gamma1 (30-55 Hz), gamma2 (60-
323 115 Hz), gamma3 (125-175 Hz), and gamma4 (185-300 Hz). Fig. 4a shows the coherence
324 spectrum across different frequency bands in WT adult MD and juvenile CPMD mice. Coherence
325 values near 1 signify all the LFP signals are synchronized at the same oscillation frequency, while
326 coherence value near zero signifies all the LFP signals are not synchronized at the same oscillation
327 frequency (Borjigin et al. 2013).

328 Firstly, after 4 days of MD in WT adult and juvenile CP mice showed higher coherence (> 0.6) at
329 low frequencies (delta, theta, alpha, and beta) and high-frequency band (gamma1) (Fig. 4b-f). In
330 Fig. 4g, WT adult MD showed low coherence (< 0.5) and juvenile CPMD showed higher
331 coherence (> 0.6) at gamma 2 (high-frequency band).On the contrary, both the groups showed low
332 coherence (< 0.5) at high frequencies (gamma3, and gamma4) (Fig. 4h-i).

333 Secondly, our results show the difference in the mean coherence between the groups for specific
334 frequency bands. Significant increase in mean coherence was observed in juvenile CPMD as
335 compared to the WT adult MD in delta (juvenile CPMD vs. WT adult MD, 0.854±0.003 vs.
336 0.746±0.009, $p<0.01$), theta (juvenile CPMD vs. WT adult MD, 0.820±0.004 vs. 0.656±0.011,
337 $p<0.001$), alpha (juvenile CPMD vs. WT adult MD, 0.809±0.004 vs. 0.674±0.011, $p<0.001$) and
338 gamma2 (juvenile CPMD vs. WT adult MD, 0.609±0.001 vs. 0.495±0.002, $p<0.01$) (Fig. 4b-d,

4g). A significant decrease in mean coherence of juvenile CPMD as compared to WT adult MD was observed in gamma3 (juvenile CPMD vs. WT adult MD, 0.247±0.001 vs. 0.343±0.001, $p<0.01$) and gamma4 (juvenile CPMD vs. WT adult MD, 0.143±0.001 vs. 0.213±0.001, $p<0.05$) (Fig. 4h-i). No significant difference in mean coherence of juvenile CPMD and WT adult MD was observed in beta (juvenile CPMD vs. WT adult MD, 0.821±0.002 vs. 0.772±0.004, $p>0.05$) and gamma1 (juvenile CPMD vs. WT adult MD, 0.842±0.003 vs. 0.783±0.002, $p>0.05$) (Fig. 4e-f). Thirdly, our results show that after 4 days of MD in WT adult mice caused no significant difference in mean coherence between the IE and the CE across all eight frequency bands ; delta (IE vs. CE, 0.744±0.009 vs. 0.747±0.009, $p>0.05$), theta (IE vs. CE, 0.653±0.011 vs. 0.658±0.011, $p>0.05$), alpha (IE vs. CE, 0.672±0.011 vs. 0.677±0.011, $p>0.05$), beta (IE vs. CE, 0.770±0.004 vs. 0.773±0.004, $p>0.05$), gamma1 (IE vs. CE, 0.784±0.002 vs. 0.783±0.002, $p>0.05$), gamma2 (IE vs. CE, 0.497±0.002 vs. 0.493±0.002, $p>0.05$), gamma3 (IE vs. CE, 0.354±0.001 vs. 0.332±0.001, $p>0.05$), gamma4 (IE vs. CE, 0.228±0.000 vs. 0.199±0.000, $p>0.05$) (Fig. 4b-i). Similarly, during 4 days of MD in juvenile animals caused no significant difference in mean coherence between the IE and the CE across all eight frequency bands ; delta (IE vs. CE, 0.851±0.003 vs. 0.857±0.003, $p>0.05$), theta (IE vs. CE, 0.811±0.010 vs. 0.829±0.012, $p>0.05$), alpha (IE vs. CE, 0.802±0.010 vs. 0.817±0.010, $p>0.05$), beta (IE vs. CE, 0.814±0.003 vs. 0.828±0.002, $p>0.05$), gamma1 (IE vs. CE, 0.842±0.001 vs. 0.841±0.001, $p>0.05$), gamma2 (IE vs. CE, 0.612±0.001 vs. 0.607±0.001, $p>0.05$), gamma3 (IE vs. CE, 0.247±0.001 vs. 0.248±0.001, $p>0.05$), gamma4 (IE vs. CE, 0.140±0.000 vs. 0.145±0.000, $p>0.05$) (Fig. 4b-i). These results show a distinct coherence change between WT adult MD and juvenile CPMD, which likely reflects the occurrence of the neuroplasticity change in juvenile CPMD. Also, they are highly correlated with our results in the previous sections that MD during a CP alters the CFC and power and no significant change was

362 observed in WT adult after 4 days MD. This finding also provides an understanding of the role of
363 oscillatory synchronization in low and high-frequency ranges in the establishment of precise
364 synchronization of neuroplasticity changes in the V1.

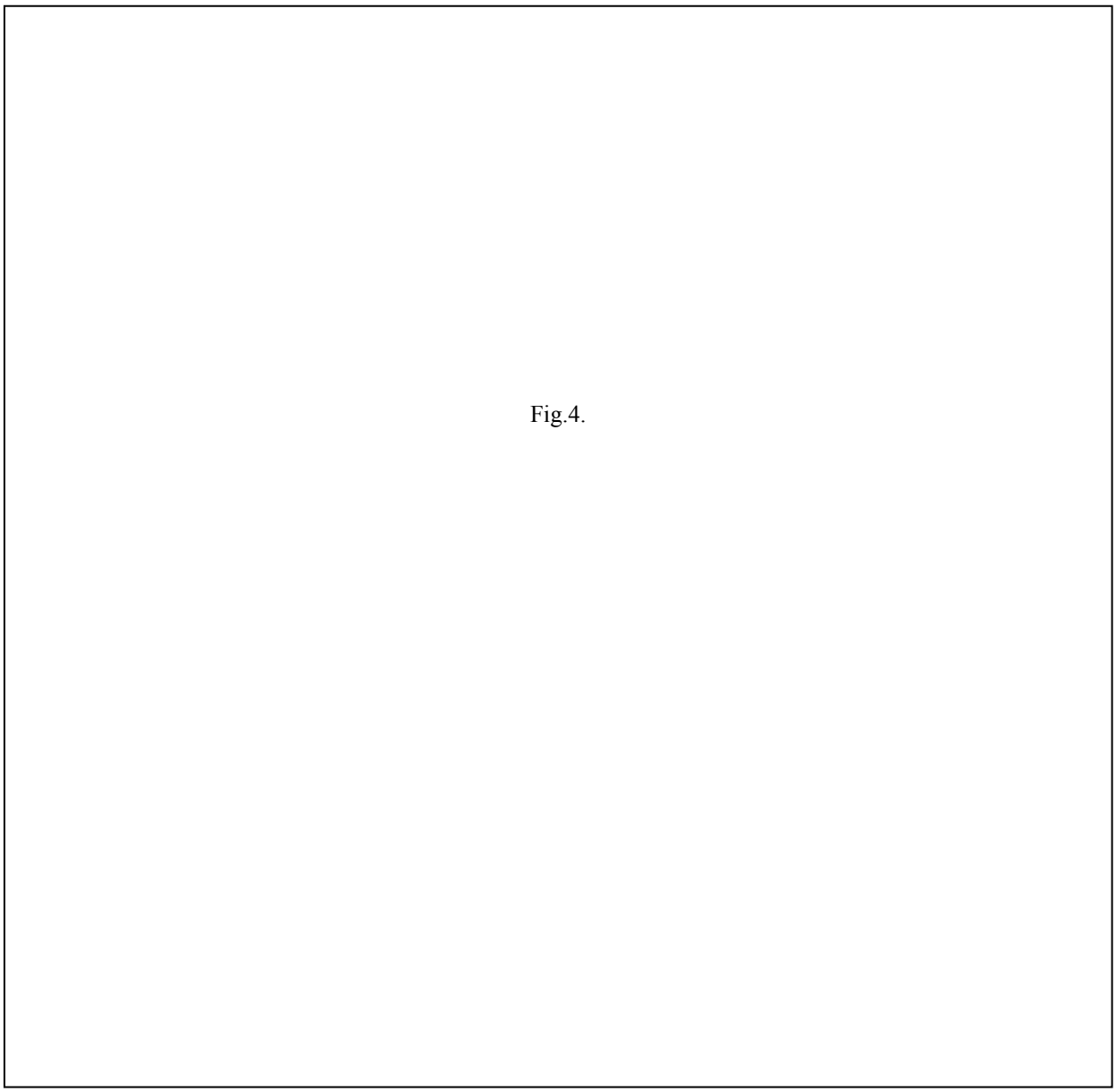

Fig.4.

365

IV. Discussion

On a neuronal time scale, the activity within and across nerve cell populations is coordinated and integrated by the rhythmic synchronisation of neurons (Engel, Fries, and Singer 2001; Fries 2015). It is assumed that neuronal rhythms are key mechanisms that facilitate perceptual processes (VanRullen 2016). Recent evidence supports the idea that phase-amplitude CFC plays a key role in the detection of sensory signals (perceptual) and cognitive and sensorimotor processing (Koster et al. 2018). The study of the coupling functions provides a new dimension and perspective regarding how the interactions between local neuronal circuits occur and manifest themselves in detail in a system. Such study determines the possibility that quantitative transitions occur between states of the composite system, e.g., via routes into and out of synchronisation, and thus play active roles in the possible self-organisation of the systems (Roopun et al. 2008a). Decomposition or alterations of the coupling functions can be used as biomarkers of change in the intrinsic properties of the neuronal circuits (Roopun et al. 2008b; Bragin et al. 1995). Research has shown that dysfunctional coupling or asynchrony is a key characteristic of several neurodegenerative and neurological diseases such as Alzheimer's disease, Parkinson's disease, schizophrenia, epilepsy, and autism (Bazzigaluppi et al. 2018; Salimpour and Anderson 2019).

Of importance to us in this study is the mice model of amblyopia, in which visual function impairment that affects one eye can be efficiently treated in adolescents but becomes irreversible in adults. This is because V1 plasticity declines dramatically at the end of the CP (Sale and Berardi 2015). Several studies have explored transient, persistent, and maintained physiological effects of CP neuroplasticity. Four days of CPMD (P23-P28) have been shown to be sufficient to induce maximal loss of responsiveness of cortical neurons to the deprived eye, leading to a shift in ocular dominance (Gordon and Stryker 1996). The effects of CPMD on the state of neuronal synchrony

of cortical oscillations in the V1 remain largely unaddressed. Therefore, the current study used LFP recordings to investigate the impact of CPMD on oscillatory synchrony in the V1 in mice models of amblyopia. Consequently, LFP signals have been studied to modulate and ultimately to re-adjust neural synchrony (Stamoulis and Richardson 2010). LFP signals enable the tracking of coupling between LFOs and HFOs.

In the present study, we explored neuronal synchrony in the amblyopia mouse model. The results showed that four days of CPMD enhanced the phase amplitude of neural oscillations. Significant enhancement of PAC of the delta oscillations with all gamma bands was observed in the IE as compared with the CE ($p<0.05$ and $p<0.01$). Also, the PAC of theta with medium and high gamma oscillations was observed in the IE as compared with the CE ($p<0.001$). In contrast, four days of MD in WT adult mice did not show any significant ($p>0.05$) enhancement of PAC between delta-gamma and theta-gamma oscillations. Our results suggest that PAC exhibits different mechanisms of neuronal processing in juvenile CPMD and WT adult MD. They indicate that PAC may represent a potential neuronal dynamic marker for CP plasticity. The experience-dependent plasticity that was induced by CPMD was characterised by the change in the coupling between low- and high-frequency synchrony. Our results demonstrate an enhanced delta-gamma and theta-gamma coupling after CPMD during adolescence, which indicates that there may be a broad range of nested oscillatory markers that are inherent to neuronal processing that is consistent with the hypothesised increase in an intrinsic coupling that arises from the neural oscillatory phase alignment. Thus, the use of LFP signals in the present study to detect changes in the strength of PAC across different states assured us that oscillatory activity plays an active role in the enablement of circuit plasticity of the V1. The relationship between neural activity and CPMD, with an interest in different oscillatory bands (delta, theta, alpha, beta, and gamma), were examined

412 in our study. The results showed that four days of CPMD significantly enhanced the delta, theta,
413 alpha, and gamma bands in the IE as compared with the CE (p<0.01 and p<0.05). In contrast, four
414 days of MD in adulthood showed significantly (p<0.05) enhanced delta and theta bands in the CE
415 as compared with the IE (p<0.05). These altered oscillations were quantified as the change in signal
416 power in specific bands and were assumed to be caused solely by neural activity changes that were
417 induced by experience-dependent plasticity in the V1.
418 In our study, to further understand the features of neural ensembles we measured the alteration in
419 coherence between populations of neurons residing at different depths in the V1 between the IE
420 and the CE in WT adult MD and juvenile CPMD mice. Coherence provides an insight into the
421 structure of communication across different layers of the V1 and how this may be influenced by
422 the MD (Buzsaki and Schomburg 2015; Srinath and Ray 2014). A higher coherence is observed
423 in juvenile CPMD at lower frequencies (delta, theta, alpha) and lower gamma frequency (gamma2)
424 while a lower coherence is observed in the juvenile CPMD at higher gamma frequencies (gamma3
425 and gamma4). Our finding shows that four days of MD enhance the mean coherence in juvenile
426 as compared to the WT adult in delta (p<0.01), theta (p<0.001), alpha (p<0.001), and gamma2
427 (p<0.01). In contrast, a significant decrease in mean coherence of juvenile CPMD as compared to
428 WT adult MD was observed in gamma3 (p<0.01), and gamma4 (p<0.05). Our results demonstrate
429 that during 4 days of MD in WT adult and juvenile animals showed no significant difference
430 (p>0.05) in mean coherence between the CE and the IE across all eight frequency bands; delta,
431 theta, alpha, beta, gamma1, gamma2, gamma3, gamma4. Our results indicate that both the eyes
432 have overlapping neurons in the V1, they produce no significant difference between the IE and the
433 CE in both WT adult MD and juvenile CPMD. However, distinct coherence change exists between
434 WT adult MD and juvenile CPMD, which likely reflects the occurrence of the neuroplasticity

change in juvenile CPMD. To the best of our knowledge, this is the first study that reveals a stronger coherence (i.e. synchronous neuronal response (Victor et al. 1994)) induced by MD at lower frequencies during experience-dependent plasticity.

In general, one of the common feature accompanied with the use of anesthesia is the suppression of high-frequency neural activity and the activation of low-frequency oscillations, as triggered by many common anesthetics (Kreuzer 2017; Brown, Lydic, and Schiff 2010). Our power spectral analysis reports the same results. In regards to the effect of K-X anesthesia on the CFC analysis increase in theta (5–10 Hz)-gamma and theta-HFO CFC in the hippocampus (Caixeta et al. 2013) and delta (1–4 Hz)-HFO CFC in the cortex and striatum (Cordon et al. 2015) are reported. Whereas, in a clinical study, ketamine does not increase frontal alpha power or induce characteristic CFC patterns between the power of alpha and the phase of slow-wave oscillations (Blain-Moraes et al. 2014). On other hand, Nase and colleagues found that in anesthetized mice, visually induced changes of cortical dynamics are evident only for beta (20-30 Hz) or low gamma (30-50 Hz) oscillations, but not for high gamma activity (Nase et al. 2003). Thus, it is likely that K-X anesthesia may contribute to visually induced neuronal oscillations during WT adult MD and juvenile CPMD, but how it contributes and how the different types of anesthesia influence our CFC results needs to be further examined in future studies.

These emergences of neural oscillations are dependent on different contributions of excitatory-inhibitory (E-I) and inhibitory-inhibitory (I-I) synaptic circuits that have been extensively studied (Stark et al. 2013; Cardin et al. 2009; Sohal et al. 2009). Cortical inhibitory interneurons play a crucial role in the maturation of visually induced beta and gamma-band oscillations during the V1 development (Morales, Choi, and Kirkwood 2002; Lazarus and Huang 2011) and their regulatory contribution to the plasticity during CP development (Hensch 2005; Espinosa and Stryker 2012).

458 In previous studies, the plasticity of the GABA population as a whole and specifically PV cells are
459 examined and found that inhibitory responses ultimately shift towards the open eye after MD
460 (Kameyama et al. 2010; Gandhi, Yanagawa, and Stryker 2008). PV cells show that MD results in
461 a rapid, but transient, reduction in PV-based inhibition, which restores PYR firing to pre-
462 deprivation levels (Kuhlman et al. 2013). Without this restoration of normal excitatory firing rates,
463 subsequent competitive plasticity will not occur. Reduction in PV-cell-evoked responses after MD
464 is restricted to the critical period for ocular dominance plasticity (ODP) and appears to be
465 necessary for the subsequent shift in excitatory ODP (Kuhlman et al. 2013). The possibility that
466 PV cells become transiently and paradoxically more responsive to the deprived eye stimulation,
467 thereby suppressing the deprived-eye response of excitatory neurons and shifting excitatory ocular
468 dominance towards the open eye as measured by the ratio of contralateral to ipsilateral eye
469 response in PV cells after brief CPMD (Yazaki-Sugiyama et al. 2009). Recent studies have also
470 suggested that PV cell activity during CPMD resulted in synchronized spontaneous activities
471 across a broad frequency band (strength of cross-frequency coupling between theta activity and
472 beta/gamma activity) (Chen et al. 2017; Bartos, Vida, and Jonas 2007). Given the existence of
473 direct or indirect connections between cortical SOM and PV cells, provides a circuit mechanism
474 by which they interact with each other to exert distinct and coordinated functions in synchronized
475 cortical oscillations. Together SOM and PV cells drive low and high-frequency oscillations (Miao
476 et al. 2016; Pfeffer et al. 2013). Thus, it is likely that this V1 inhibitory circuit could be fundamental
477 for the regulation of neuronal oscillations and synchronization between LFOs and HFOs during
478 CPMD. In addition to the enrolment of cortical local inhibitory interneurons, brief monocular
479 deprivation during CP downregulates neuregulin-1(NRG1)/ErbB4 signaling in PV neurons,
480 causing retraction of excitatory inputs to PV neurons (Sun et al. 2016; Kuhlman et al. 2013). The

molecular mechanism underlying is exogenous NRG1 rapidly restores excitatory inputs onto deprived PV cells through downstream PKC-dependent activation and AMPA receptor exocytosis, thus enhancing PV neuronal inhibition to excitatory neurons. Thus, it might be another mechanism be involved in the emergence of the visually included delta, theta, and gamma-band cross-coupling oscillations in developing V1 during the CP.

CONCLUSION

Mismatch of the input to the brain from the eyes during CPMD may activate ensembles of neuronal cells in a highly asynchronous manner, giving rise to strong delta-gamma and theta-gamma oscillations that drive the plasticity process. Our results demonstrate high-frequency activity that is coupled to low-frequency phase synchrony during CPMD, with features that suggest neuroplasticity-related mechanisms. The present study opens the door to a deepened understanding of the functional role of experience-dependent plasticity on phase-amplitude coupling.

ACKNOWLEDGMENT

This work was supported by the City University of Hong Kong (SRG-Fd 7005452, 7005632) and the Hong Kong Research Grants Council (RGC) General Research Fund Grant 11208218, 11207419 (CityU 9042648, 9042829).

References

Antonini A, Fagiolini M, and Stryker MP. 1999. Anatomical correlates of functional plasticity in mouse visual cortex, J Neurosci, 19: 4388-406.

Bartos M, Vida I, and Jonas P. 2007. Synaptic mechanisms of synchronized gamma oscillations in inhibitory interneuron networks, Nat Rev Neurosci, 8: 45-56.

Bazzigaluppi P, Beckett TL, Koletar MM, Lai AY, Joo IL, Brown ME, Carlen PL, McLaurin J, and Stefanovic B. 2018. Early-stage attenuation of phase-amplitude coupling in the hippocampus and medial prefrontal cortex in a transgenic rat model of Alzheimer's disease, J Neurochem, 144: 669-79.

Berens P, Keliris GA, Ecker AS, Logothetis NK, and Tolias AS. 2008. Comparing the feature selectivity of the gamma-band of the local field potential and the underlying spiking activity in primate visual cortex, Front Syst Neurosci, 2: 2.

Blain-Moraes S, Lee U, Ku S, Noh G, and Mashour GA. 2014. Electroencephalographic effects of ketamine on power, cross-frequency coupling, and connectivity in the alpha bandwidth, Front Syst Neurosci, 8: 114.

Bonnefond M, and Jensen O. 2015. Gamma activity coupled to alpha phase as a mechanism for top-down controlled gating, PLoS One, 10: e0128667.

Borjigin J, Lee U, Liu T, Pal D, Huff S, Klarr D, Sloboda J, Hernandez J, Wang MM, and Mashour GA. 2013. Surge of neurophysiological coherence and connectivity in the dying brain, Proc Natl Acad Sci U S A, 110: 14432-7.

Bragin A, Jando G, Nadasdy Z, Hetke J, Wise K, and Buzsaki G. 1995. Gamma (40-100 Hz) oscillation in the hippocampus of the behaving rat, J Neurosci, 15: 47-60.

Brown EN, Lydic R, and Schiff ND. 2010. General anesthesia, sleep, and coma, N Engl J Med, 363: 2638-50.

Bruns A, and Eckhorn R. 2004. Task-related coupling from high- to low-frequency signals among visual cortical areas in human subdural recordings, Int J Psychophysiol, 51: 97-116.

Buzsaki G, and Draguhn A. 2004. Neuronal oscillations in cortical networks, Science, 304: 1926-9.

Buzsaki G, and Schomburg EW. 2015. What does gamma coherence tell us about inter-regional neural communication?, Nat Neurosci, 18: 484-9.

Caixeta FV, Cornelio AM, Scheffer-Teixeira R, Ribeiro S, and Tort AB. 2013. Ketamine alters oscillatory coupling in the hippocampus, Sci Rep, 3: 2348.

Canolty RT, Edwards E, Dalal SS, Soltani M, Nagarajan SS, Kirsch HE, Berger MS, Barbaro NM, and Knight RT. 2006. High gamma power is phase-locked to theta oscillations in human neocortex, Science, 313: 1626-8.

Cardin JA, Carlen M, Meletis K, Knoblich U, Zhang F, Deisseroth K, Tsai LH, and Moore CI. 2009. Driving fast-spiking cells induces gamma rhythm and controls sensory responses, Nature, 459: 663-7.

Chen G, Rasch MJ, Wang R, and Zhang XH. 2015. Experience-dependent emergence of beta and gamma band oscillations in the primary visual cortex during the critical period, Sci Rep, 5: 17847.

Chen G, Zhang Y, Li X, Zhao X, Ye Q, Lin Y, Tao HW, Rasch MJ, and Zhang X. 2017. Distinct Inhibitory Circuits Orchestrate Cortical beta and gamma Band Oscillations, Neuron, 96: 1403-18 e6.

Cordon I, Nicolas MJ, Arrieta S, Lopetegui E, Lopez-Azcarate J, Alegre M, Artieda J, and Valencia M. 2015. Coupling in the cortico-basal ganglia circuit is aberrant in the ketamine model of schizophrenia, Eur Neuropsychopharmacol, 25: 1375-87.

Demiralp T, Bayraktaroglu Z, Lenz D, Junge S, Busch NA, Maess B, Ergen M, and Herrmann CS. 2007. Gamma amplitudes are coupled to theta phase in human EEG during visual perception, Int J Psychophysiol, 64: 24-30.

Engel AK, Fries P, and Singer W. 2001. Dynamic predictions: oscillations and synchrony in top-down processing, Nat Rev Neurosci, 2: 704-16.

Espinosa JS, and Stryker MP. 2012. Development and plasticity of the primary visual cortex, Neuron, 75: 230-49.

Fagiolini M, Pizzorusso T, Berardi N, Domenici L, and Maffei L. 1994. Functional postnatal development of the rat primary visual cortex and the role of visual experience: dark rearing and monocular deprivation, Vision Res, 34: 709-20.

Fries P. 2015. Rhythms for Cognition: Communication through Coherence, Neuron, 88: 220-35.

Gandhi SP, Yanagawa Y, and Stryker MP. 2008. Delayed plasticity of inhibitory neurons in developing visual cortex, Proc Natl Acad Sci U S A, 105: 16797-802.

Gao R. 2016. Interpreting the electrophysiological power spectrum, J Neurophysiol, 115: 628-30.

Gordon JA, and Stryker MP. 1996. Experience-dependent plasticity of binocular responses in the primary visual cortex of the mouse, J Neurosci, 16: 3274-86.

557 Guire ES, Lickey ME, and Gordon B. 1999. Critical period for the monocular deprivation effect in rats: assessment
558 with sweep visually evoked potentials, J Neurophysiol, 81: 121-8.
559 Henrie JA, and Shapley R. 2005. LFP power spectra in V1 cortex: the graded effect of stimulus contrast', J
560 Neurophysiol, 94: 479-90.
561 Hensch TK. 2005. Critical period plasticity in local cortical circuits, Nat Rev Neurosci, 6: 877-88.
562 Issa NP,Trachtenberg JT, Chapman B, Zahs KR, and Stryker MP. 1999. The critical period for ocular dominance
563 plasticity in the Ferret's visual cortex, J Neurosci, 19: 6965-78.
564 Kameyama K, Sohya K, Ebina T, Fukuda A, Yanagawa Y, and Tsumoto T. 2010. Difference in binocularity and
565 ocular dominance plasticity between GABAergic and excitatory cortical neurons, J Neurosci, 30: 1551-9.
566 Katzner S, Nauhaus I, Benucci A, Bonin V, Ringach DL, and Carandini M. 2009. Local origin of field potentials in
567 visual cortex, Neuron, 61: 35-41.
568 Koster M, Finger H, Graetz S, Kater M, and Gruber T. 2018. Theta-gamma coupling binds visual perceptual features
569 in an associative memory task, Sci Rep, 8: 17688.
570 Kreuzer M. 2017. EEG Based Monitoring of General Anesthesia: Taking the Next Steps, Front Comput Neurosci, 11:
571 56.
572 Kuhlman SJ, Olivas ND, Tring E, Ikrar T, Xu X, and Trachtenberg JT. 2013. A disinhibitory microcircuit initiates
573 critical-period plasticity in the visual cortex, Nature, 501: 543-6.
574 Lakatos P, Karmos G, Mehta AD, Ulbert I, and Schroeder CE. 2008. Entrainment of neuronal oscillations as a
575 mechanism of attentional selection, Science, 320: 110-3.
576 Lazarus MS, and Huang ZJ. 2011. Distinct maturation profiles of perisomatic and dendritic targeting GABAergic
577 interneurons in the mouse primary visual cortex during the critical period of ocular dominance plasticity, J
578 Neurophysiol, 106: 775-87.
579 Lensjo KK, Lepperod ME, Dick G, Hafting T, and Fyhn M. 2017. Removal of Perineuronal Nets Unlocks Juvenile
580 Plasticity Through Network Mechanisms of Decreased Inhibition and Increased Gamma Activity, J Neurosci,
581 37: 1269-83.
582 Miao Q, Yao L, Rasch MJ, Ye Q, Li X, and Zhang X. 2016. Selective Maturation of Temporal Dynamics of
583 Intracortical Excitatory Transmission at the Critical Period Onset, Cell Rep, 16: 1677-89.
584 Morales B, Choi SY, and Kirkwood A. 2002. Dark rearing alters the development of GABAergic transmission in
585 visual cortex, J Neurosci, 22: 8084-90.
586 Nase G, Singer W, Monyer H, and Engel AK. 2003. Features of neuronal synchrony in mouse visual cortex, J
587 Neurophysiol, 90: 1115-23.
588 Pfeffer CK, Xue M, He M, Huang ZH, and Scanziani M. 2013. Inhibition of inhibition in visual cortex: the logic of
589 connections between molecularly distinct interneurons, Nat Neurosci, 16: 1068-76.
590 Rasch MJ, Gretton A, Murayama Y, Maass W, and Logothetis NL. 2008. Inferring spike trains from local field
591 potentials, J Neurophysiol, 99: 1461-76.
592 Roopun AK, Kramer MA, Carracedo LM, Kaiser M, Davies CH, Traub RD, NJ Kopell, and Whittington MA. 2008a.
593 Period concatenation underlies interactions between gamma and beta rhythms in neocortex, Front Cell
594 Neurosci, 2: 1.
595 Roopun AK, Kramer MA, Carracedo LM, Kaiser M, Davies CH, Traub RD, NJ Kopell, and Whittington MA. 2008b.
596 Temporal Interactions between Cortical Rhythms, Front Neurosci, 2: 145-54.
597 Sale A, and Berardi N. 2015. Active training for amblyopia in adult rodents, Front Behav Neurosci, 9: 281.
598 Salimpour Y, and Anderson WS. 2019. Cross-Frequency Coupling Based Neuromodulation for Treating Neurological
599 Disorders, Front Neurosci, 13: 125.
600 Sawtell NB, Frenkel MY, Philpot BD, Nakazawa K, Tonegawa S, and Bear MF. 2003. NMDA receptor-dependent
601 ocular dominance plasticity in adult visual cortex, Neuron, 38: 977-85.
602 Sohal VS, Zhang F, Yizhar O, and Deisseroth K. 2009. Parvalbumin neurons and gamma rhythms enhance cortical
603 circuit performance, Nature, 459: 698-702.
604 Srinath R, and Ray S. 2014. Effect of amplitude correlations on coherence in the local field potential, J Neurophysiol,
605 112: 741-51.
606 Stamoulis C, and Richardson AG. 2010. Encoding of brain state changes in local field potentials modulated by motor
607 behaviors, J Comput Neurosci, 29: 475-83.
608 Stark E, Eichler R, Roux L, Fujisawa S, Rotstein HG, and Buzsaki G. 2013. Inhibition-induced theta resonance in
609 cortical circuits, Neuron, 80: 1263-76.
610 Sun Y, Ikrar T, Davis MF, Gong N, Zheng X, Luo ZD, Lai C, Mei L, Holmes TC, Gandhi SP, and Xu X. 2016.
611 Neuregulin-1/ErbB4 Signaling Regulates Visual Cortical Plasticity, Neuron, 92: 160-73.

612 Tagawa Y, Kanold PO, Majdan M, and Shatz CJ. 2005. Multiple periods of functional ocular dominance plasticity in
613 mouse visual cortex, Nat Neurosci, 8: 380-8.
614 Tort AB, Komorowski R, Eichenbaum H, and Kopell N. 2010. Measuring phase-amplitude coupling between neuronal
615 oscillations of different frequencies, J Neurophysiol, 104: 1195-210.
616 VanRullen R. 2016. Perceptual Cycles, Trends Cogn Sci, 20: 723-35.
617 Victor JD, Purpura K, Katz E, and Mao B. 1994. Population encoding of spatial frequency, orientation, and color in
618 macaque V1, J Neurophysiol, 72: 2151-66.
619 Whittingstall K, and Logothetis NK. 2009. Frequency-band coupling in surface EEG reflects spiking activity in
620 monkey visual cortex, Neuron, 64: 281-9.
621 Yazaki-Sugiyama Y, Kang S, Cateau H, Fukai T, and Hensch TK. 2009. Bidirectional plasticity in fast-spiking GABA
622 circuits by visual experience, Nature, 462: 218-21.
623
624
625
626
627
628
629
630
631
632
633
634
635
636
637
638
639
640
641

642 **Caption to table**

643 Table 1. Effect of monocular deprivation in (WT) wild-type adult and juvenile C57BL/6 mice on
644 the delta-gamma and theta-gamma phase-amplitude couplings.

	WT Adult MD (P60-P65)			**Juvenile CPMD (P23-P28)**		
	IE	CE	*p*	IE	CE	*p*
Delta-gamma	4.555±0.525	4.504±0.406	>0.05	6.634±0.400	4.722±0.226	<0.01
Theta-gamma	0.058±0.000	0.051±0.000	>0.05	4.597±0.035	2.543±0.021	<0.01

645 Values are mean ± SEM of phase-amplitude coupling (PAC) normalized by 10^{-3}. *p* values are given for comparison
646 between the IE & the CE. IE, ipsilateral eye and CE, contralateral eye.

647
648
649
650
651
652
653
654
655
656
657
658
659
660
661
662
663

664
665
666
667
668
669
670

671 **Captions to figures**

672 Fig. 1. Demonstration of electrophysiological recording from different layers of the visual cortex
673 (V1). A polyimide-coated platinum/iridium ribbon microelectrode array (16-channel) was used to
674 record the local field potential signals (LFPs) from the binocular zone of the V1. The LFPs were
675 recorded from the different layers of the V1. Optimal stimuli were presented to each eye
676 alternately, and the relative strength of the responses was determined.

677

678 Fig. 2. Effect of monocular deprivation (MD) in adult and juvenile C57BL/6 mice across low-
679 frequency (delta (0.5-5 Hz) and theta (5-10 Hz)) and high-frequency (gamma (30-300 Hz)) bands.
680 Fig. (*a*) and (*b*) show the comodulogram which indicates the modulation index as heat map. (*a*),
681 The negligible difference is seen in the ipsilateral eye (IE) and the contralateral eye (CE) in WT
682 adult MD on delta-gamma and theta-gamma plots. (*b*), In juvenile CPMD, a difference is observed
683 between the IE and the CE on delta-gamma (dotted white box) and theta-gamma (dotted black
684 box) plots. Fig. (*c*) and (*d*) show the mean modulation index between low frequency (delta and
685 theta) and high frequency (gamma1, gamma2, gamma3, and gamma4). (*c*), No significant
686 difference is observed between the IE and the CE in WT adult MD on delta-gamma and theta-
687 gamma (n.s., $p>0.05$). (*d*), In juvenile CPMD, a significant difference is observed between the IE

and the CE on delta-gamma1 (**p<0.01), delta-gamma2 (**p<0.01), delta-gamma3 (**p<0.01), delta-gamma4 (*p<0.05), theta-gamma2 (***p<0.001), and theta-gamma3 (***p<0.001). No significant difference is seen in the IE and the CE on theta-gamma1 (n.s., p>0.05) and theta-gamma4 (n.s., p>0.05). Error bars in this study indicate the standard error of the mean (SEM).

Fig. 3. Effect of monocular deprivation (MD) on spontaneous local field potential (LFPs) power in WT adult and juvenile C57BL/6 mice across different frequency ranges, i.e. delta (0.5-5 Hz), theta (5-10 Hz), alpha (10.5-15 Hz), beta (15-30 Hz), and gamma (30-300 Hz). LFP power (mean power ± SEM) at delta frequency is compared between the ipsilateral eye (IE) and the contralateral eye (CE) in WT adult MD and juvenile CPMD. (*a*), A significant difference (*p<0.05) is observed in both groups. LFP power (mean power ± SEM) at theta frequency is compared between the IE and the CE in adult MD and juvenile CPMD. (*b*), A significant difference in both the groups, WT adult MD (*p<0.05) and juvenile CPMD (**p<0.01) is observed. LFP power at the alpha frequency (mean power ± SEM) is compared between the IE and the CE in WT adult MD and juvenile CPMD. (*c*), No significant difference in WT adult MD (n.s., p>0.05) and significant difference in juvenile CPMD (**p<0.01) is observed. LFP power at the beta frequency (mean power ± SEM) is compared between the IE and the CE in WT adult MD and juvenile CPMD. (*d*), No significant difference (n.s., p>0.05) is observed in both groups. LFP power at gamma frequency (mean power ± SEM) is compared between the IE and the CE in WT adult MD and juvenile CPMD. (*e*), No significant difference in WT adult MD (n.s., p>0.05) and a significant difference in juvenile CPMD (**p<0.01) is observed. Error bars in this study indicate the standard error of the mean (SEM). Mean power is expressed in decibels (dB).

Fig. 4. Effect of monocular deprivation on spontaneous local field potential (LFPs) mean coherence in adult and juvenile C57BL/6 mice across different frequency ranges, namely delta (0.5-5 Hz), theta (5-10 Hz), alpha (10.5-15 Hz), beta (15-30 Hz), and gamma1 (30-55 Hz), gamma2 (60-115 Hz), gamma3 (125-175 Hz), and gamma4 (185-300 Hz). Results represent the mean coherence ± SEM across all frequency bands. (*a*), LFP coherence spectrum across different frequency bands in WT adult MD and juvenile CPMD mice. Coherence at delta frequency is compared between the ipsilateral eye (IE) and the contralateral eye (CE) in WT adult MD and juvenile CPMD. (*b*), No significant difference (n.s., $p>0.05$) is observed in both eyes in the same groups. A significant difference between WT adult MD and juvenile CPMD (**$p<0.01$) is observed. Coherence at theta frequency is compared between the IE and the CE in WT adult MD and juvenile CPMD. (*c*), No significant difference (n.s., $p>0.05$) is observed in both eyes in the same groups. A significant difference between WT adult MD and juvenile CPMD (***$p<0.001$) is observed. Coherence at alpha frequency is compared between the IE and the CE in WT adult MD and juvenile CPMD. (*d*), No significant difference (n.s., $p>0.05$) is observed in both eyes in the same groups. A significant difference between WT adult MD and Juvenile CPMD (***$p<0.001$) is observed. Coherence at beta frequency is compared between the IE and the CE in WT adult MD and juvenile CPMD. (*e*), No significant difference (n.s., $p>0.05$) is observed in both eyes in the same groups. No significant difference between WT adult MD and juvenile CPMD (n.s., $p>0.05$) is observed. Coherence at gamma1 frequency is compared between the IE and the CE in WT adult MD and juvenile CPMD. (*f*), No significant difference (n.s., $p>0.05$) is observed in both eyes in the same groups. No significant difference between WT adult MD and juvenile CPMD (n.s., $p>0.05$) is observed. Coherence at gamma2 frequency is compared between the IE and the CE in WT adult MD and juvenile CPMD. (*g*), No significant difference (n.s., $p>0.05$) is

observed in both eyes in the same groups. A significant difference between WT adult MD and juvenile CPMD (**p<0.01) is observed. Coherence at gamma3 frequency is compared between the IE and the CE in WT adult MD and juvenile CPMD. (*h*), No significant difference (n.s., p>0.05) is observed in both eyes in the same groups. A significant difference between WT adult MD and juvenile CPMD (**p<0.01) is observed. Coherence at gamma4 frequency is compared between the IE and the CE in WT adult MD and juvenile CPMD. (*i*), No significant difference (n.s., p>0.05) is observed in both eyes in the same groups. A significant difference between WT adult MD and juvenile CPMD (*p<0.05) is observed. Error bars in this study indicate the standard error of the mean (SEM).

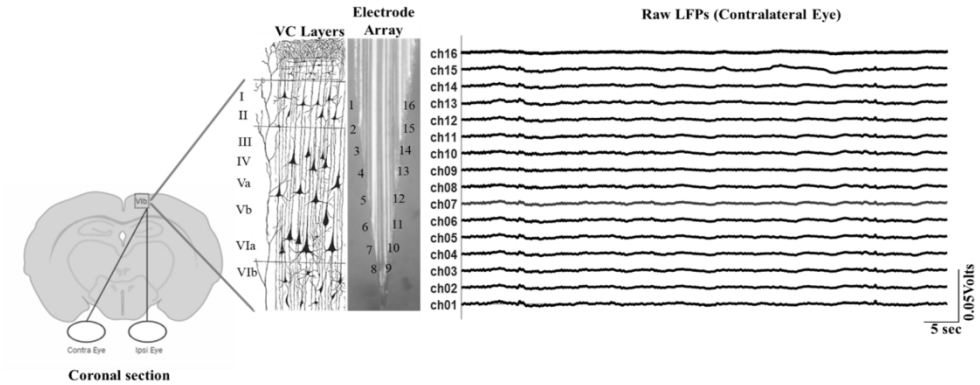

Fig. 1

320x138mm (150 x 150 DPI)

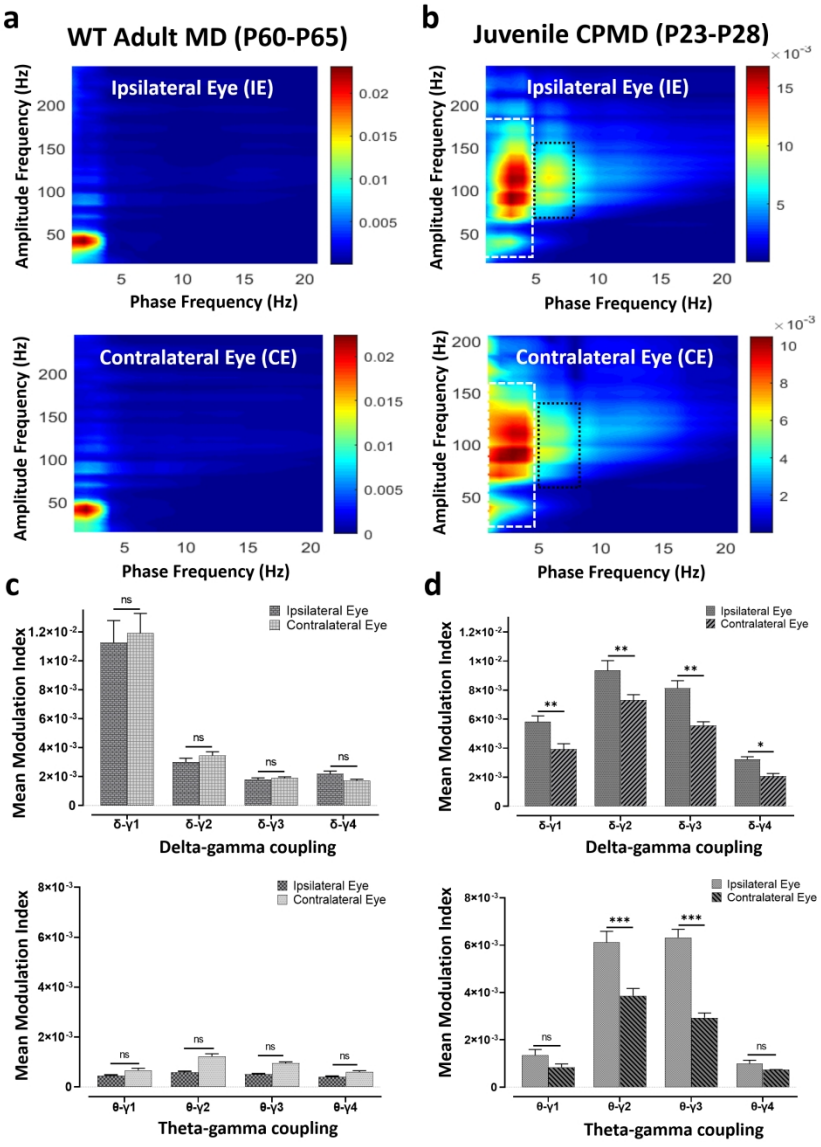

Fig. 2

417x534mm (150 x 150 DPI)

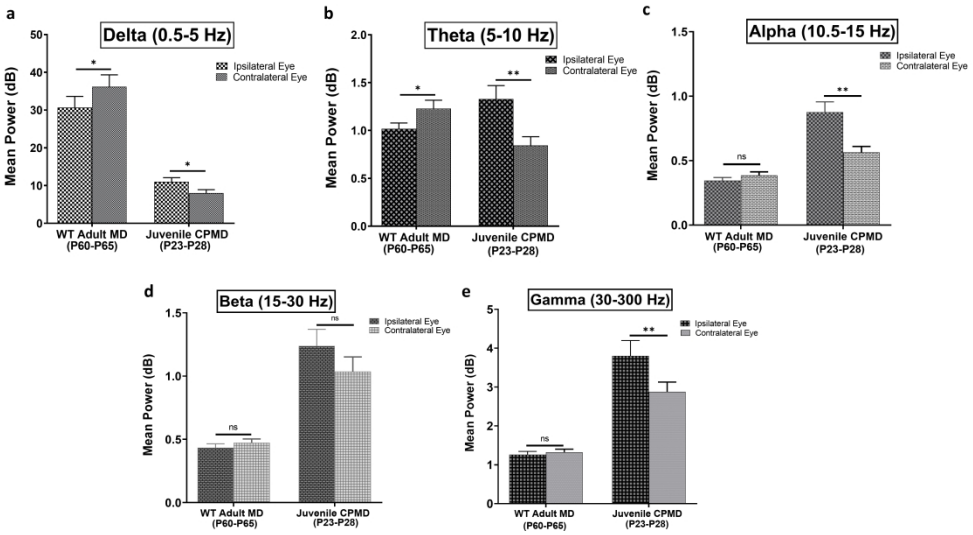

Fig. 3

853x485mm (150 x 150 DPI)

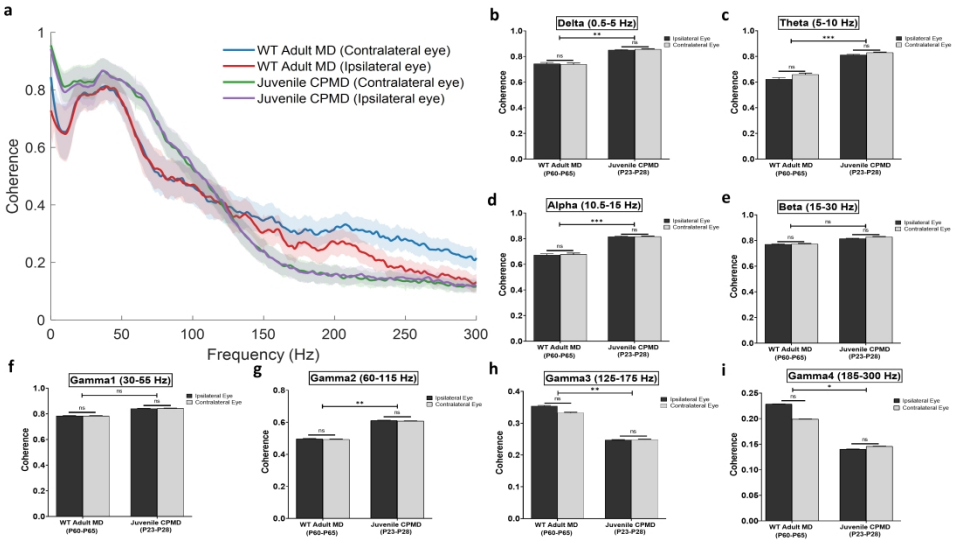

Fig. 4

866x514mm (150 x 150 DPI)